Assembling reconfigurable endoluminal surgical systems: opportunities and challenges

Z. Nagy*, M. Flückiger, R. Oung, I.K. Kaliakatsos, E.W. Hawkes and B.J. Nelson

Institute of Robotics and Intelligent Systems,
ETH Zurich, Tannenstr 3, Zürich, 8092 Switzerland
E-mail: nagyz@ethz.ch   E-mail: michael.flueckiger@alumni.ethz.ch
E-mail: roung@ethz.ch   E-mail: ikaliakatsos@ethz.ch
E-mail: ewhawkes@gmail.com E-mail: bradley.nelson@iris.mavt.ethz.ch
*Corresponding author

K. Harada

CRIM Laboratory, Scuola Superiore Sant'Anna,
Viale Rinaldo Piaggio 34, Pontedera, Pisa, Italy
E-mail: k.harada@sssup.it

E. Susilo, A. Menciassi and P. Dario

CRIM Laboratory, Scuola Superiore Sant'Anna,
Viale Rinaldo Piaggio 34, Pontedera, Pisa, Italy
and
Italian Institute of Technology (IIT) Network,
Via Morego 30, Genova, 16163 Italy
E-mail: ekawahyu@crim.sssup.it
E-mail: arianna.menciassi@sssup.it
E-mail: paolo.dario@sssup.it

J.J. Abbott

Department of Mechanical Engineering,
University of Utah,
50 S. Central Campus Dr.,
Salt Lake City, Utah, 84112, USA
E-mail: jake.abbott@utah.edu

Abstract: The success of capsule endoscopy has promoted the development of the next generation of endoluminal surgical devices, and many research groups have proposed robotic capsules with novel functionalities, such as active locomotion and surgical intervention capabilities. Yet, these capsules are still single robotic units with a limited number of components and degrees of freedom. This paper addresses this inherent limitation of single capsule units by introducing the concept of modular robotics for surgical robotics. In the proposed procedure, the modules are ingested and assembled in the stomach cavity. We report on the key technologies of such a system: its self-assembly, actuation, power, and localisation.

Keywords: biomedical robotics; self-assembly; self-reconfiguration; robotic capsules.

Biographical notes: Zoltan Nagy received his Dipl.Ing (MS) in Mechanical Engineering at ETH Zurich in 2006. He is a PhD candidate at the Institute of Robotics and Intelligent Systems at ETH Zürich. His research interests include modular robotics and biomedical robotics.

Michael Flückiger received his Dipl.Ing (MS) in Mechanical Engineering from ETH Zurich in 2004, and his PhD in Sciences from ETH Zurich in 2009. He is currently working as an Engineer at HBI in Bern, Switzerland.

Raymond Oung received his BSc in Electrical Engineering at the University of Toronto, Canada in 2006. He received his MSc in Mechanical Engineering at the ETH Zurich, Switzerland in 2008. Since 2008, he has been working towards his PhD at the Institute of Dynamic Systems and Control (IDSC) at ETH Zurich. His main research interests include distributed estimation and a controls and modular robotics.

Ioannis K. Kaliakatsos received his Dipl.Ing. in Mechanical Engineering from the National Technical University of Athens, Greece, in 2006. The same year he joined the Institute of Robotics and Intelligent Systems at ETH Zurich as a PhD candidate. He is interested in wireless powering methods for pipe inspection vehicles.

Elliot W. Hawkes graduated at the Harvard University with Highest Honours in 2009 with a BSc in Mechanical Engineering. He was awarded both the National Defence Science and Engineering Graduate Fellowship and the National Science Foundation Graduate Fellowship in 2009. His interests include mesoscale robotics.

Bradley J. Nelson received his PhD in Robotics from Carnegie Mellon University in 1995. He was an Assistant Professor at the University of Illinois at Chicago, Associate Professor at the University of Minnesota, and became Full Professor at ETH Zurich in 2002. His primary research direction lies in extending robotics research into emerging areas of science and engineering. He has been a finalist for and/or won best paper awards at major robotics conferences and journals in 2004, 2005, 2006, 2007, 2008 and 2009. He was named to the 2005 'Scientific American 50,' Scientific American magazine's annual list recognizing outstanding acts of leadership in science and technology for his work in nanotube manufacturing.

Kanako Harada received her BE and MS in Precision Machinery Engineering from The University of Tokyo and her PhD in Engineering from Waseda University in 1999, 2001 and 2007, respectively. After working for Hitachi, Ltd., she became a Visiting Research Associate of Waseda University. She worked for the National Center for Child Health and Development, Japan from July 2005. Since April 2007, she is a Postdoctoral Research Fellow in the CRIM Lab of Scuola Superiore Sant'Anna, Italy. Her research interests are in the field of surgical robotics.

Ekawahyu Susilo received his Bachelors in Electrical Engineering from the Universitas Surabaya, Indonesia in July 2000. Six months later he joined Universitas Surabaya and is working as a Lecturer since then. During four years time, he had been the Head of Automation Laboratory in the same university and also the Head of Microcontroller Division in School of Technology (SofT) in Surabaya, Indonesia. In 2009, he received his PhD from the Scuola Superiore Sant'Anna, Pisa, Italy in the field of Bioengineering. His major interests are in real time embedded system, embedded system design and robotic applications. He has received many awards in scientific writings and robotic contests.

Arianna Menciassi received her Laurea degree in Physics (with Honours) from the University of Pisa (Italy) in 1995. She obtained her PhD from the Scuola Superiore Sant'Anna (SSSA, Pisa, Italy) in 1999 with a research program on the micromanipulation of mechanical and biological micro objects. Currently she is a Professor of Biomedical Robotics at SSSA. Her main research interests are in the fields of biomedical micro- and nano-robotics, microfabrication technologies, micromechatronics and microsystem technologies. She is working on several European projects and international projects for the development of micro- and nano-robotic systems for medical applications.

Paolo Dario received his Laurea degree in Mechanical Engineering from the University of Pisa (Italy) in 1977. He has been a Visiting Professor at the Ecole Polytechnique Federale de Lausanne (EPFL) and at Waseda University, Tokyo. He is a Professor of Biomedical Robotics at the Scuola Superiore Sant'Anna (SSSA), Pisa. He is the Founder and Director of the BioRobotics Laboratories of SSSA (about 80 researchers). His research interests are in medical robotics, mechatronics and microengineering. He is a member of the Board of the International Foundation of Robotics Research and he served as President of the IEEE Robotics and Automation Society.

Jake J. Abbott received his PhD in Mechanical Engineering from the Johns Hopkins University, Baltimore, MD, in 2005. He became a Postdoctoral Research Associate at the Institute of Robotics and Intelligent Systems, ETH Zurich, Switzerland, in 2005, and an Assistant Professor at the University of Utah, Salt Lake City, UT, in 2008. He is currently the Head of the Telerobotics Laboratory, Department of Mechanical Engineering, University of Utah, where his research involves medical and microscale telerobotics.

1 Introduction

Capsule endoscopy is now widely accepted and has contributed to the early diagnosis of pathologies in the gastrointestinal (GI) tract. This success of capsule endoscopy has promoted the development of the next generation of endoluminal surgical devices – endoluminal devices that perform not only imaging of the internal wall of the GI tract but also intensive examination and intervention in the very early stages of the pathologies. In order to enhance the dexterity of the conventional endoscopic capsules, active locomotion of the capsule have been studied, such as legged capsules (Quirini et al., 2008), capsules driven by using external magnetic fields (Sendoh et al., 2003), and swimming capsules with propellers (Carta et al., 2008). Moreover, endoscopic devices with high dexterity and interventional capabilities (Abbott et al., 2007; Lehman et al., 2008) have been developed for natural orifice translumenal endoscopic surgery (NOTES). The dexterity and function of those advanced surgical devices are, however, not sufficient because the number of components and degrees of freedom that can be implemented in one surgical unit is limited. To overcome the inherent limitation of a single robotic unit, an assembling reconfigurable endoluminal surgical (ARES) system is proposed (ARES, 2009, http://www.ares-nest.org) to introduce the concept of modular robotics into surgical robotics. The proposed surgical procedures using this kind of system are shown in Figure 1.

In the proposed procedures, miniaturised robotic modules are ingested and assembled in the stomach cavity. Thus, the size of a module should be such that it is ingestible, and at least as small as the current commercial capsule endoscopes (11 mm in diameter and 26 mm in length). During the assembly procedure, the stomach cavity can be filled with a liquid to distend the stomach up to 1.4 litre and to aid in the self-assembly of the robotic modules either in the liquid or on its surface. The assembly needs to be completed before the liquid naturally drains away, which is in 10–20 minutes. The assembled robot can change its configuration according to the target location and target task, while the position of each module is monitored by a localisation system and the robotic structure is manoeuvred via wireless bidirectional communication with an external console operated by the surgeon.

After the surgical task in the stomach cavity is completed, the robot might completely disassemble into individual modules. Or, it could also reconfigure itself into another topology, e.g., into a snake-type structure, and move on to examine, for example, the small intestine, which cannot be reached by an endoscope. A possible application in this case would be the detection of bleeding sites in the small intestine.

Owing to the modular scheme of ARES, various surgical instruments can be brought into the GI tract, and the instruments can be used cooperatively to perform complicated surgical tasks with high accuracy. Extra modules can be added later to the robotic structure, even

during the operation. Moreover, broken modules and the modules that are not necessary in subsequent procedures can be detached and discarded or replaced with other ones.

Figure 1 ARES procedure
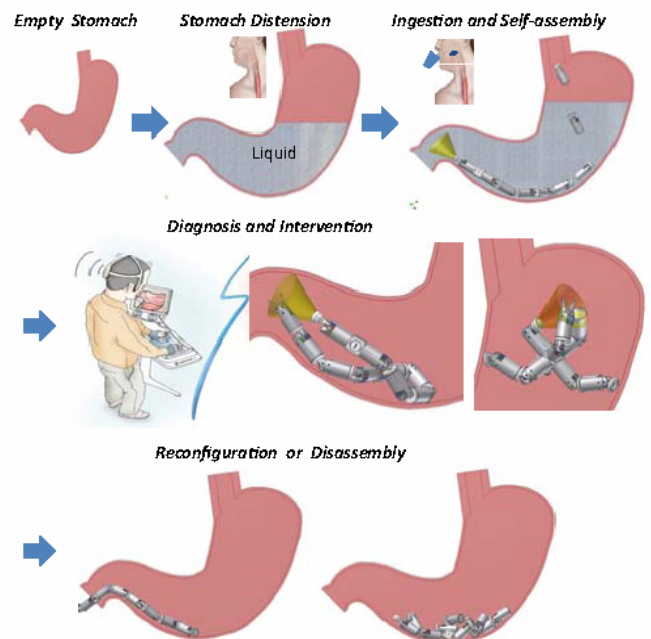
The concept of the abovementioned ARES system is innovative and has potential for use in next-generation medical applications. Among many technologies necessary to realise the ARES system, primary key technologies are identified as self-assembly, actuation, power, and localisation. In this paper, several approaches toward each of these technologies are proposed with preliminary results, specifically considering the feasibility and challenges of system integration. After careful validation of each of the technical components, the principle conclusion of this work is that the proposed integrated system for clinical use is technically feasible.
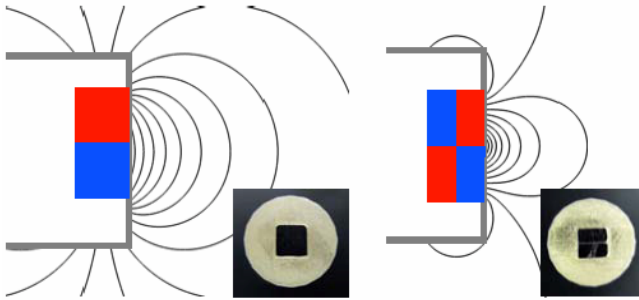
2 Self-assembly

The fundamental challenge for the success of the ARES concept is the self-assembly of the modules. Due to their long-range passive interaction, the use of magnets as the driving mechanism of self-assembly seems self-evident: if magnets are placed on the mating faces, the magnetic force will attract the different modules toward each other and the magnetic torque will orient them. In addition, magnets provide a reversible connection allowing for disconnection and reconfiguration. However, it is not evident what magnetic configuration (i.e., number and orientation of the magnets) to use in order to achieve the highest probability for a successful connection. It is desirable that each module is able to connect to any other module to increase the number of possible topologies of the robot, and that the mating faces connect in a unique orientation to enable *a*

priori design of the possible kinematic configurations without the need for additional position/orientation sensors.

For a unique connection, the mating faces should present exactly two opposite magnetic poles, resulting in a magnetic self-aligning hermaphroditic (MASH) mating face. The two conceivable realisations, as shown in Figure 2, are with one magnet oriented such that the connection takes place along an axis perpendicular to the magnetisation of the magnet (MASH-1), and with two distinct magnets (MASH-2). Experiments with upscaled models of single MASH-1 mating faces under quasi-static conditions, as well as magnetic field analysis, suggested that the MASH-1 configuration is useful for self-assembly and alignment (Nagy et al., 2007). However, due to the dynamic and random nature of the assembly process, experiments under more realistic conditions were necessary to investigate which configuration provides superior self-assembly.

Figure 2   Field plots of the (left) MASH-1 (right) MASH-2 (right) configurations


Note: The insets show actual prototype modules used in the experiments.

During self-assembly, the modules move such that the free energy of the system is minimised. Due to the large number of forces involved (gravity, magnetic force/torque between the modules, fluid drag on the modules, the friction between touching modules, and the friction between the modules and the GI-tract wall), as well as the randomness of initial conditions, multiple local energy minima are present. Thus, in addition to the desired successfully connected state, other states are possible ranging from misaligned assembly to no interaction at all. No numerical tools are available to capture all of the above physical effects in a single simulation. Therefore, we have developed a set of simple modules to abstract the problem of self-assembly and study it experimentally. An analysis of the involved magnetic forces and torques is provided by Nagy et al. (2008).

We consider cylindrical modules with length 7 mm (short) and 14 mm (long) and diameter 9 mm. These sizes are chosen such that three small modules fit into a ConiSnap R capsule of size 000 (length 26.1 mm, outer diameter 9.5 mm), and the long modules having twice the length of the short ones [see Figures 3(a), 3(b)]. In addition to size 000, the DBAAA sized capsules (length 23 mm, outer diameter 11 mm) are also conceivable as carriers for robot modules. As the two capsules are the largest commercially

available, they represent an approximate upper limit of such modules. By using modules of this size, we expect no significant scaling effects.

Figure 3   (a) A long module in a DBAAA-sized module (b) three short modules in a 000 sized capsule (c, d, e) parallel, perpendicular, and antiparallel orientation
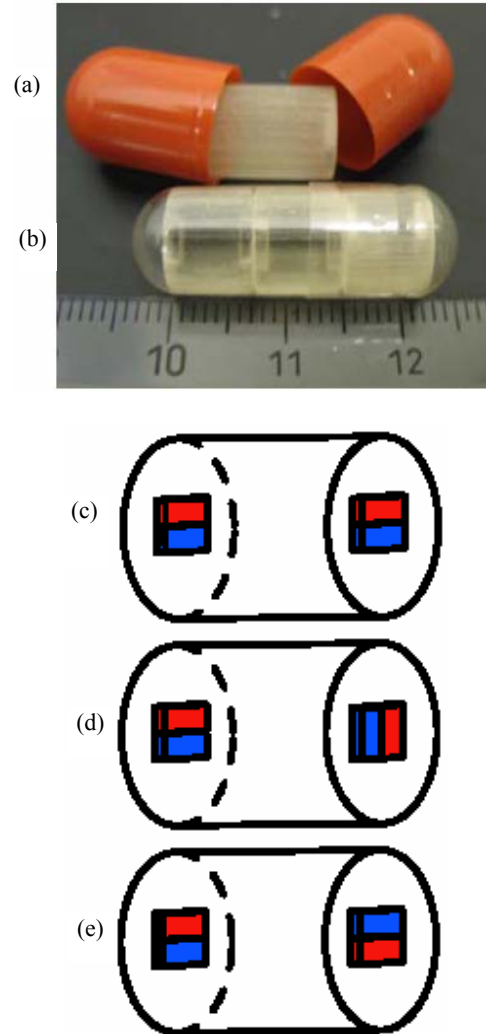
Note: Only MASH-1 modules are shown for simplicity.

The modules are fabricated out of an acrylic-based photopolymer by rapid prototyping, and permanent magnets are glued into the designated openings at both ends of the modules. We explore three different possible arrangements of the magnets on a given module, as shown in Figures 3(c)–3(e): parallel, perpendicular, and antiparallel. The orientation is not significant for the short range interaction between two modules (for the sizes and magnets investigated in this work), because the shape of the magnetic field is locally dominated by a single MASH face. In the long range, on the other hand, the field is shaped by both MASH faces. Therefore, an influence of the orientation is expected. For the MASH-1 configuration, one 3 mm × 3 mm × 1 mm magnet is used on each face, whereas for the MASH-2 configuration, two 3 mm × 1.5 mm× 1 mm

magnets are used. The result is a 3 mm × 3 mm magnetic face with a depth of 1 mm for both MASH types (see insets in Figure 2). The magnets are NdFeB magnets with a remanence of 1.4 T.

The self-assembly performance for a given design is investigated by the following experiment: first, from a given location, one module is dropped into a receptacle filled with a cup of water (≈ 300 mL). The water simulates the water that is consumed by the patient when swallowing the pills. After having waited for the first module to settle, the second module is dropped from the same position but at a random orientation. Two different receptacles are used: a tapered bowl (height 75 mm, upper diameter 120 mm, lower diameter 50 mm), as well as an anatomically correct model of a dilated stomach (volume 1.4 L) milled out of acrylic glass (Figure 4). The stomach model has a preferred direction and a curved bottom, allowing us to study the self-assembly process at scale. Using the bowl allows us to draw more general conclusions.

Figure 4 Stomach model used for the self-assembly experiments

For each configuration, 50 drops are performed and the percentage of successful connections is recorded, as are the different misalignments that occurred. In total, we observed seven different states: the successful connection (S), five stable misalignments (1–5), and a no-interaction state (X) [see Figure 5(a)]. Figure 5(b) shows the experimental results. We observed that MASH-1 modules show significantly higher success rates that the MASH-2 modules, and that long modules tend to assemble better than short ones.

Depending on the actual task of the robot, some of the misaligned states can be considered as successful connections. For example, State 3 is kinematically similar to the (most stable) success state. In addition, States 2, 4, and 5 have been observed to be comparatively unstable and little excitation caused them to reorient into either State 3 or the success state. Such an excitation can be provided by applied magnetic fields, palpation, or the peristaltic motion of the stomach. Under these considerations, the self-assembly success rate would be greatly improved.

Figure 5 (a) Observed stable states during the drop experiments: successful connection (S) and five misalignments (15) (b) results of the drop experiments

(a)*

(b)
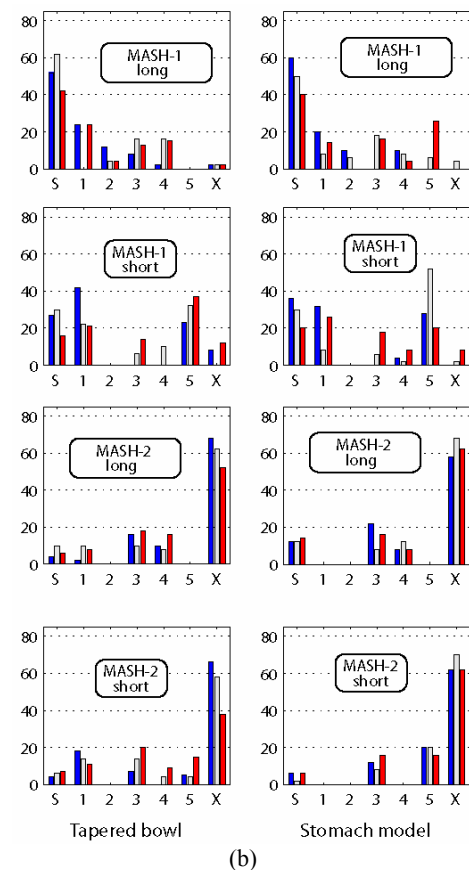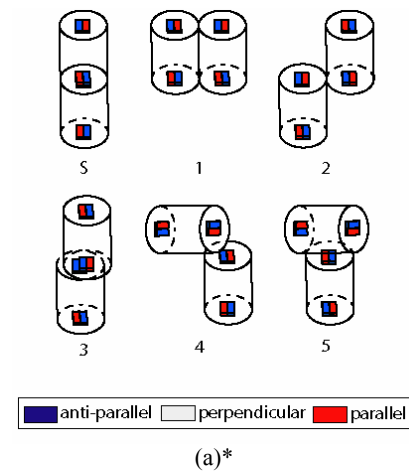
Notes: *Only antiparallel MASH-1 modules are shown, the states for the other modules are comparable.
**The percentage occurrence of the different states is shown. The no-interaction state is indicated by X. Clearly, for both the short and the long modules, the MASH-1 configuration provides a much higher success rate than the MASH-2 modules. In addition, very few no-interaction states are observed with MASH-1.

It is possible to increase the self-assembly performance by optimising the size of the MASH-1 magnets relative to the size of the modules. We performed the drop experiment with long MASH-1 modules with 4 mm × 4 mm × 2 mm sized magnets oriented perpendicularly. For the bowl, this increased the success rate to 74%. Furthermore, States 3 and 4 were reduced to 8% and 10% respectively, and the no-interaction state was not observed at all. As in the previous experiment with the smaller magnets, States 1 and 5 did not occur. However, State 2 occurred twice as often as before (8%). For the stomach model, the larger magnets resulted in the same success rate of 74%, eliminated States 3 and 5, and reduced the States 1 and 2 to both 4%. Only State 4 was increased to 18%.

Of course, for a successful intervention of the ARES robot, the kinematic configuration has to be determined accurately. This is possible if a 100% success rate for the self-assembly can be guaranteed, or if feedback on the assembly state is available. A simple method for such a feedback are Hall effect sensors, often employed for measuring magnetic fields. Once information on the kinematic structure is available, the robotic surgery can be planned, even for non-ideally assembled configurations. To increase the success rate itself, several parameters are available. The magnet size and shape has to be optimised with respect to actual geometry and inertia of the modules. Magnets that are too small do not guarantee sufficiently high interaction forces, whereas large magnets might induce undesirable yet stable misalignments. Shaping the geometry of the mating face, while still maintaining its hermaphroditic nature, will change the frictional behaviour and will allow the misaligned states to reorient into the successful connected state. Note also, that the magnetic field of the MASH-1 faces can be shaped by introducing soft-magnetic shielding material near the magnet to guide its flux, with the potential to reduce the occurrence of misalignments. Finally, externally applied magnetic fields allow for guided self-assembly, reducing to some extend the random nature of the assembly process, thus making it more predictable.

Clearly, our experiments simplify the real process, in that the stomach wall properties and the peristaltic motion of the stomach are neglected. However, the stomach wall is rather slippery, therefore minimal friction effects are expected. Furthermore, the motion of the stomach adds external energy to the whole self-assembly system, allowing it to potentially reconfigure from an undesirable into a more stable desirable configuration. To conclude, even though the real stomach properties are neglected, the obtained statistical results help to build intuition on magnetic self-assembly.

3   Actuation

After successful self-assembly, the robot requires actuated degrees of freedom for functionality. This includes locomotion, intervention, and eventual disassembly. Given the target size of the ARES modules, we are pursuing two potential actuation schemes in parallel. First, using miniaturised DC motors and transmissions, and second, using smart materials, such as shape memory alloys (SMA).

3.1   Motors and transmissions

The use of commercial components enables quick fabrication of the prototypes, and available peripheral devices make the integration of the total system easier. In particular, the miniaturised brushless DC motors with high gear ratios from Namiki Precision Jewel Co., Ltd., Japan, produce very high torque, and the size is acceptable for ingestible devices. From the company, both a 2.4 mm motor (SBL02-06H1PG337: the gear ratio is 337:1, the diameter is 2.4 mm, the length is 10.8 mm including the gear head, and the stall torque is 0.69 mNm) and a 4 mm motor (SBL04-0829PG337: the gear ratio is 337:1, the diameter is 4.0 mm, the length is 17.4 mm including the gear head, and the stall torque is 10.6 mNm) are available. Since the motor driver board for these motors (SSD04, Namiki Precision Jewel Co., Ltd., 19.6 mm× 34.4 mm × 3 mm) has an inappropriate size for ingestible devices, a new control board (9.6 mm in diameter, 2.5 mm of thickness, and weight of 0.37 g) was designed and developed in-house using commercially available components, as described in Susilo et al. (2008). This new board was built using a CC2430 microcontroller (Texas Instrument, USA) and three sets of A3901 dual bridge motor drivers (Allegro MicroSystem, Inc., USA) to control the motor. The A3901 motor driver chip was originally intended for a brushed DC motor, but a software commutation algorithm was implemented so that it could control a brushless DC motor as well. An IEEE 802.15.4 wireless personal area network (WPAN) was also introduced as an embedded feature of the microcontroller. This implemented algorithm enables the control of the selected brushless DC motor in back electro-motive force (BEMF) feedback mode or slow speed stepping mode. With the stepping mode, the motor can be driven with a resolution of 0.178° although the eventual resolution of the actuation depends on the precision of other structural components as well. Owing to the high gear reduction of the motor itself (337:1), the motor can maintain its position even when there is no current flowing.

By using the abovementioned motors and the developed control board, structural modules have been designed as detailed in Harada et al. (2008) and Menciassi et al. (2008). Figure 6 shows one of the module designs and Figure 7 shows the resulting fabricated prototype. The designed structural module has two degrees of freedom (±90° of bending and 360° of rotation), and it contains a Li-Po battery (20 mAh, LP2-FR, Plantraco Ltd., Canada), two brushless DC motors (SBL04-0829PG337), and the motor control board in an acrylic plastic casing fabricated by a 3D printing machine (Invison XT 3-D Modeler, 3D systems, Inc., USA). The nylon gears used for the mechanisms were purchased from DIDEL (DIDEL SA, Switzerland) and modified by additional machining afterwards. Two permanent magnets (Q-05-1.5-01-N, Webcraft GMbH, Switzerland) are attached at each end of the module to help

with self-alignment and modular docking. These magnets will be replaced with the ones chosen by the self-assembly study described in the previous section. The overall module size is 15.4 mm in diameter and 36.5 mm in length, the weight is 5.6 g, and the plan is to further miniaturise it.

Figure 6 Design of the structural module
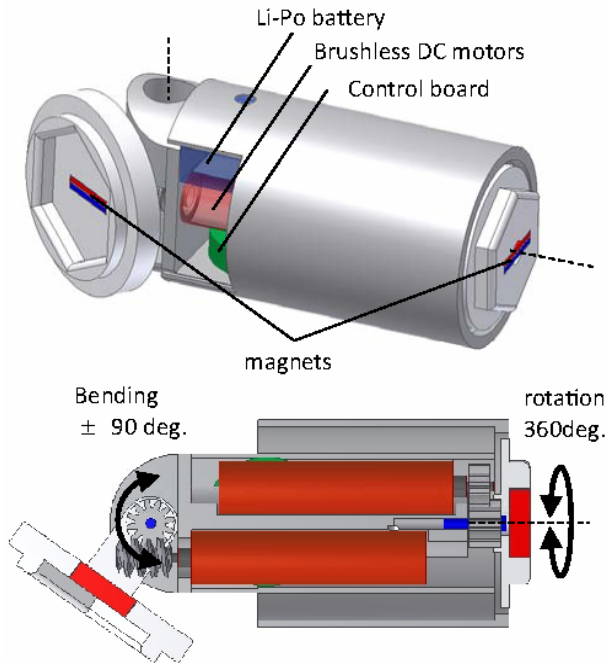
Figure 7 Components and a prototype of the structural module


3.2 SMA and flexures

Due to their biocompatibility, large displacement capabilities, and favourable scaling behaviour, we chose SMA wires (NiTi) coiled into springs as potential actuators for the ARES modules. SMA return to their memorised shape upon heat application due to the phase transition from martensite to austenite. During this transition, recovery of about 4−5% of deformation strain, without hysteresis effects are possible. Coiling SMA wires into linear springs further increases their large displacement capability and allows the

design of customisable and scalable actuators. The typical drawbacks of SMA actuators – low bandwidth, slow response time, and high power consumption – become less important on downscaling as detailed in Peirs et al. (1998). We used 100 μm thick wires, and for the heat application, we chose DC Joule heating due to its simplicity.

Because SMA wires are one-way actuators, a restoring mechanism is required. This can be implemented using conventional springs. However, this requires that the conventional spring's spring constants lies between the austenite and the martensite spring constant of the SMA spring. At the envisaged scales, this limits the design of the SMA springs and thus their potential. Therefore, we designed actuators with antagonistic SMA springs, i.e., when one SMA is actuated (contracted), the other one is passively expanded and will be contracted during the next actuation cycle.

The linear actuator is shown in Figure 8. In this sliding piston-like mechanism, the SMA springs are fixed on the piston and routed through the central column, and act to move the piston through it. The frame of the actuator is fabricated by rapid prototyping (stereo lithography) and the shaft is made of aluminium.

Figure 8 Linear actuator
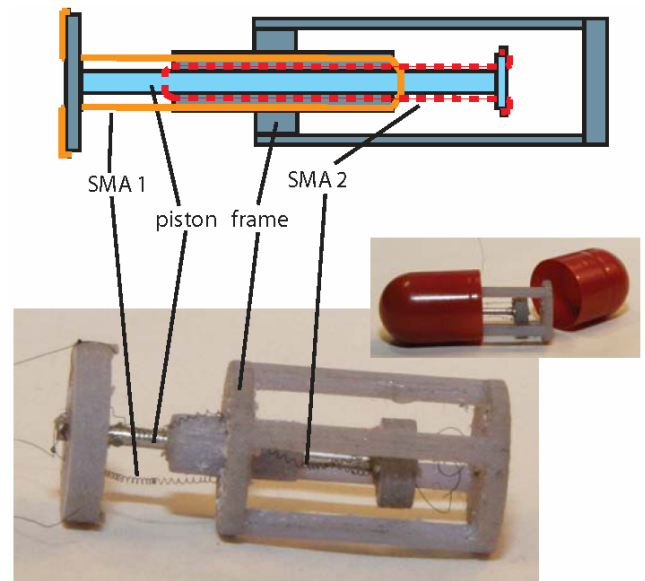
Note: See text for explanation.

For the fabrication of a bending actuator, we used the smart composite microstructures (SCM) process proposed by Wood et al. (2008) for the design of robots with characteristic dimensions in the order of mm. The process allows the integration of rigid links and large angle flexure joints through a laser micromachining and lamination process. See Hoover et al. (2008) for an example of the SCM process, where an autonomous crawling hexapod robot, 3 cm in length, and with 57 joints, has been implemented.

Figure 9(a) shows the design of our bending actuator. It consists of two main body parts composed of three rigid

segments (glass fibre) and two flexures (Dupont Kapton) about 1 mm wide and 100 µm thick , fabricated by the SCM process and glued (with two component epoxy glue) to a circular part (also glass fibre) at each end. The SMA springs are attached to a raised point on these circles and rapid prototyped stoppers were glued on the body parts to limit the bending of either joint to ±45°. If two modules are attached to each other with such an actuator, the bending angle at their connecting joint will be ±90°. Two pivots at the end of the module instead of one in the centre [Figure 9(b)] allow it to use the space between the SMAs and the rigid link, e.g., for electronics. See Figure 9(c) for the final device.

**Figure 9**   Bending actuator

(a)

(b)
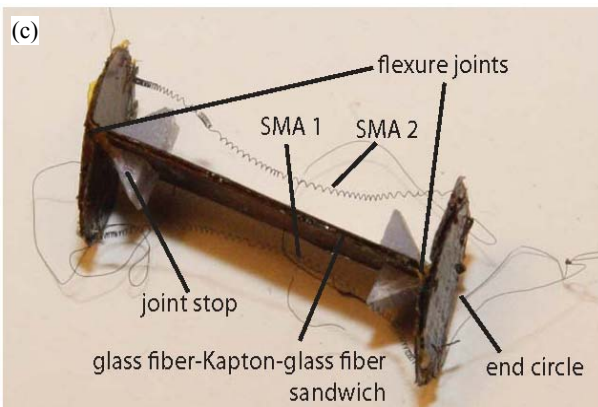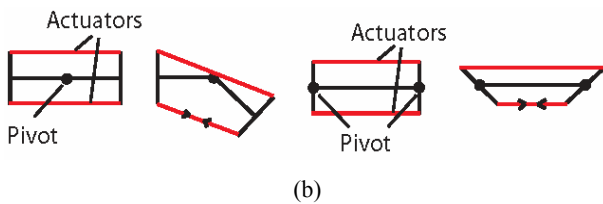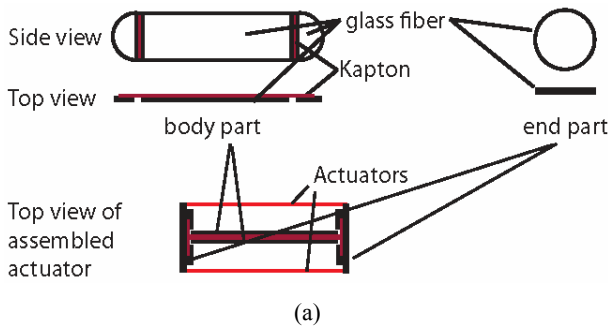
Note: See text for explanation.

3.3   *Design of a disconnection mechanism*

For a modular robot, a mechanism that allows one module to disconnect from another one is desirable. Disconnecting two magnets typically requires that they are translated with respect to each other, and the force that is applied has to be larger than the magnetic force that holds the magnets together. For MASH-type connectors, another mechanism is

available: rotating the magnets with respect to each other. This not only reduces the holding force, but for rotation angles larger than 90°, the force changes from attraction to repulsion, effectively acting as a disconnecting force. In addition, rotating a magnet requires significant less space than translating it, making this solution particularly interesting in our case. We designed and implemented an actuator that has a bending joint similar to the one presented above, and an additional rotational joint with the magnet attached to it, see Figure 10. The basic parts of the device are the body, the columns, the braces, the top, and the rotor. The columns are attached to the body by a Kapton flexure and provide the bending motion. They, in turn, support the top, to which the bending actuators are attached. The top is prevented from simply flopping from side to side by the braces, and thus all pieces move together in relation to the body as the bending actuators fire. Between the two columns, the rotor is suspended by Kapton, rotating in and out of the page with respect to the body. The magnet is mounted to the rotor, centred under the top. Two actuators span from the free end of the rotor, down either side, to the column with which it is joined. These create the rotation necessary to detach one module from the next, if they are attached top to top. See the support material for a demonstration of the disconnection process.

Figure 10   Disconnection mechanism
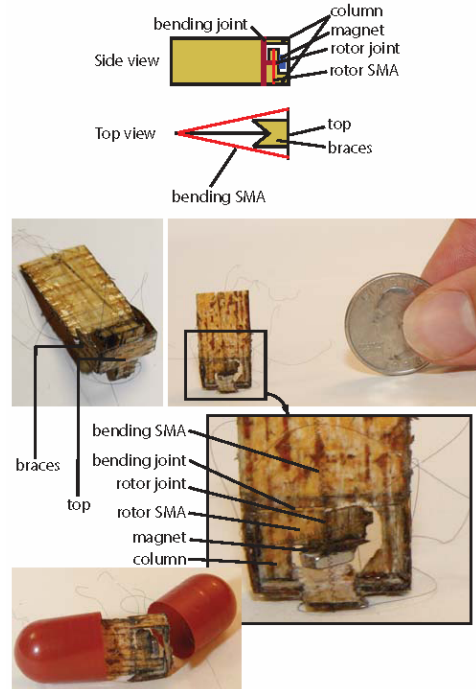
During the design processes, emphasis was laid on limiting the power consumption of the SMAs to realistic values. For a single actuation stroke, we achieved a power consumption of less than 200 mW, which is state-of-the-art in wireless power transfer for capsule type devices (see Section 4). Together with on-board electronics and batteries, the

presented actuators offer a promising technology for swallowable robots.

4 Power

The most straightforward approach for powering the ARES modules is to use onboard batteries similar to capsule endoscopes. This requires each module to carry its own battery pack, and thus significantly reduces the available volume for payload and tools. An alternative approach is electromagnetic induction, which has been studied for its potential application in endoscopic capsules. Following Faraday's law, an electric potential V is induced in a coil of wire when the magnetic flux Φ enclosed by it varies with time (see Figure 11):

$$V = \frac{d\Phi}{dt} = -\frac{d}{dt}\int_s \mathbf{B}.d\mathbf{S} \tag{1}$$

Figure 11 Principle of electromagnetic induction used to wirelessly power microrobots
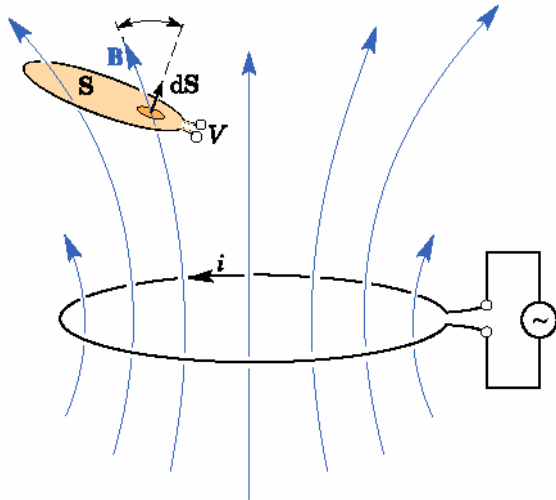
Notes: The change of magnetic flux, generated by current i, induces the voltage V. The flux is maximised when **B** and d**S** are parallel.

The emission and reception of flux is typically performed by a simple pair of coils. To power the ARES robot externally, the emitter coil would be placed outside the human body and the receiver coils inside of a module. Under this scheme, there are no size constraints on the emitter coil, in contrast to the modules, which must be small enough to be ingested. The main source of voltage degradation is misalignment between emitter and receiver, as the angle between **B** and d**S** in Figure 11 indicates. When the two vectors are parallel, flux attains its maximum value. To eliminate this sensitivity in orientation, additional coils in mutually perpendicular planes can be installed, either on the emitter or the receiver side. With such configurations, Lenaerts and Puers (2005) reported power transfer of 150 mW usable DC power, and Ryu et al. (2007) achieved

300 mW power transfer. These numbers show that the power requirements for the SMA actuators presented in the previous sections can be met.

In the modular scheme of the ARES robot, it is conceivable that only one or a few modules are powered. Such 'power modules' could receive power wirelessly and use it to charge up the on-board battery and/or to provide peak power additionally to the battery when necessary. To power other modules in this scenario, power transfer from one module to another is necessary. Again, induction can be used, since in the assembled robot the mating faces of two adjacent modules are close to each other and aligned. If coils are placed close to the surface of the connecting faces of the modules, a large amount of the flux emitted by one coil can be captured by the other one. In addition, information can also be transferred between modules in this way, as shown in Catrysse et al. (2004). In order to experimentally investigate this method, we created the pair of coils shown in Figure 12(a). The circuit schematic is shown in Figure 12(b). The coils have 21 turns (three layers with seven turns per layer), an external diameter of 10 mm, a width of 3 mm, and they are placed 0.6 mm apart. The diameter value is typical of commercial capsule endoscopes. The inductance of the coils was measured as 4.65 μH. The load on the receiver side was assumed to be a pure resistor RL. Two capacitors of 0.22 μF were used to tune the resonant frequency of the circuits; on the emitter side the capacitor was placed in series with the coil, while on the receiver side in parallel. This means the receiver side will behave like a voltage source. The resonant frequency calculated by $\omega_0 = 1/\sqrt{LC}$ is 157.4 kHz.

A sinusoidal voltage of frequency f was given as input to the emitter circuit. By changing the frequency of the voltage, and by measuring the input voltage amplitude V_0, the input current amplitude i_0 and phase θ, and the resistor voltage amplitude V_L, we determined the power transfer efficiency defined as

$$\eta = \frac{V_L^2/2R_L}{\left(V_0/\sqrt{2}\right)\left(i_0/\sqrt{2}\right)\cos\theta} = \frac{V_L^2/R_L}{V_0 i_0 \cos\theta} \tag{2}$$

that is, as the ratio of the average DC power that is reaching the resistor load over the average DC power consumed by the emitter circuit. The results for $R_L = 10\,\Omega$ can be seen in Figure 12(c), where a maximum experimental efficiency of 48.66% was observed at 155 kHz, corresponding well with the predicted resonance frequency. It is clear that the maximum efficiency depends on the value R_L of the load as can be also seen in Figure 12(c) where a $910\,\Omega$ resistor load was used. In that case, the maximum efficiency dropped to 4.87% but the frequency at which resonance occurred remained unaffected. For our given test circuit, an optimisation analysis revealed that the load that maximises the power transfer efficiency is $10.98\,\Omega$ and that this maximum efficiency is $\eta_{max} = 49.95\%$ (Figure 13).

Figure 12 (a) Experimental setup used to investigate power transfer from one module to another (b) its schematic. R_1 and L_1 are the coil resistance and self inductance, respectively, and C_1 is the compensating capacitor. The same holds for the receiver circuit (subscript 2). R_L is the resistor load. (c) Experimentally obtained efficiency versus input voltage frequency for a 10 Ω and 910 Ω load
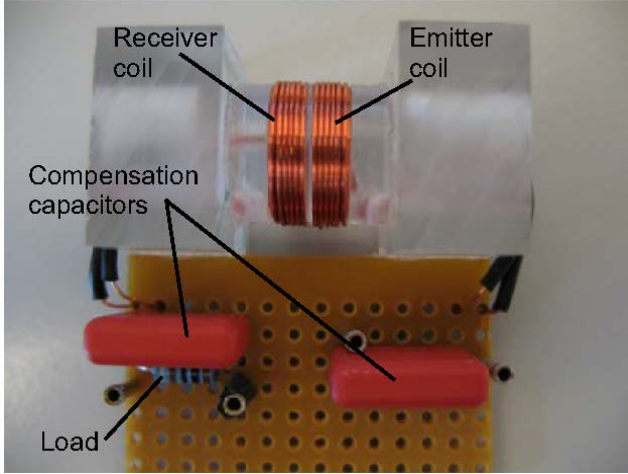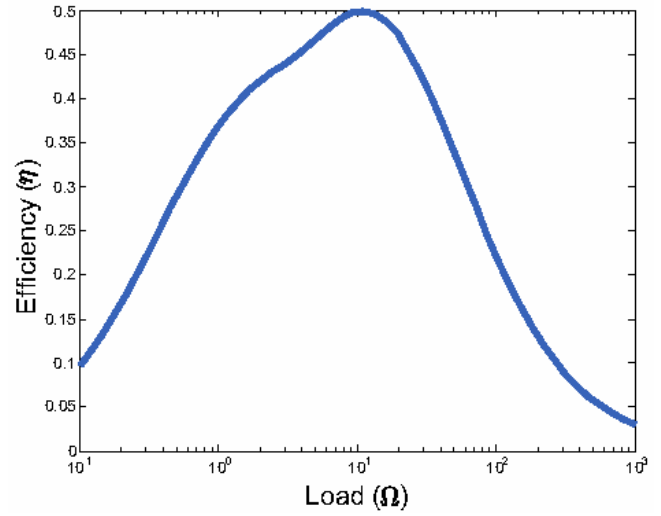

(a)
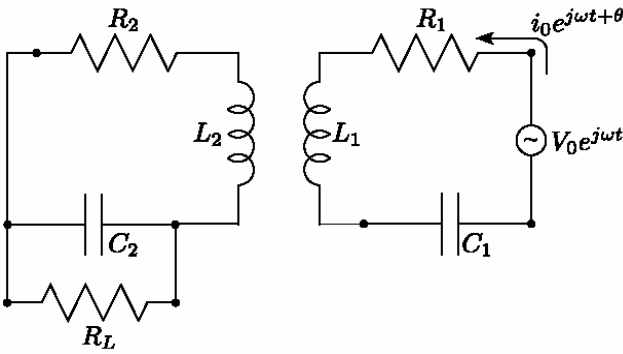
(b)
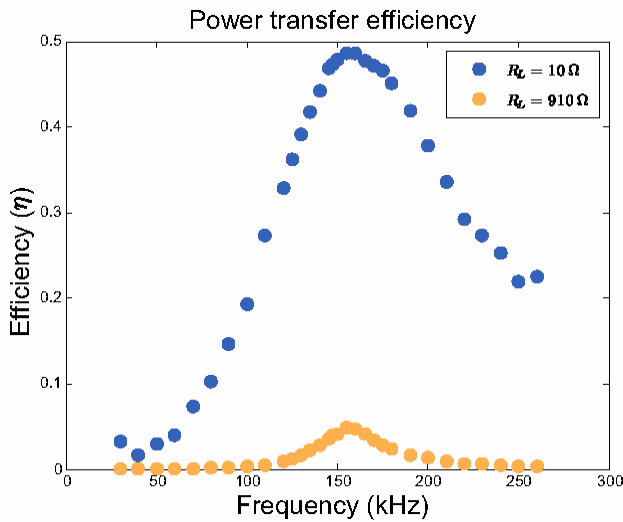
(c)

Figure 13 Maximum efficiency as a function of resistor load for the setup shown in Figure 12(a)

Induction is not the only viable means of wireless power transfer using magnetic fields. An alternative method of powering microdevices is to use piezoelectric and magnetostrictive materials in a laminate configuration as suggested by O'Handley et al. (2008). The magnetostrictive layers embrace a piezoelectric sheet and when they are exposed to an alternating magnetic field they change their dimensions. This exerts pressure on the intermediate piezoelectric material and thus voltage is generated.

5   Localisation

While procedures in the stomach do not necessarily require localisation of the robot, for interventions in other parts of the GI tract, e.g., the intestine, it is desirable, if not required, to correlate position information with sensor data, such as camera images.

Minimally, invasive surgical localisation comes in many forms, such as endoscopy, magnetic resonance, computed tomography, positron emission tomography, and ultrasound. Wells (2000) states that for the localisation in human soft tissue, only ultrasound among these techniques combines good resolution, minimal adverse health effects, high-speed, adequate frame rates, and low cost.

Flückiger and Nelson (2007) proposed a new passive localisation method that utilises ultrasonic time difference of arrival (TDOA) measurements for the accurate localisation of an ultrasound emitter, like an ultrasonically marked capsule, inside of the human body.

The localisation of the capsule is performed by spatially separated receivers combined into an array and placed around the volume of interest, as shown in Figure 14. The receivers capture the ultrasound signal coming from an emitter mounted on the capsule (ultrasonically marked item). The emitter location relative to the receiver locations is calculated by estimating the TDOA for different receiver pairs.

Figure 14 Ultrasonically marked capsule
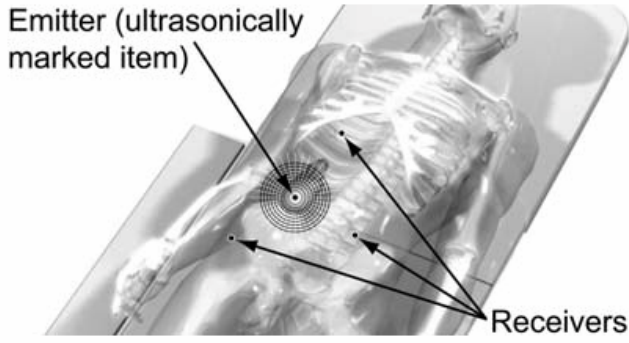
Source: Body image courtesy of HMA3d, Barnsley, UK.

Figure 15 Probability maps for the localisation of an emitter obtained from two receivers, (a) hyperbolic areas for the emitter location in 2-D at 50 kHz if the receivers are close together (b) hyperbolic areas for the emitter location in 2-D at 50 kHz (c) hyperbolic areas for the emitter location in 2-D at 300 kHz

(a)

(b)

(c)

For a given TDOA, the emitter location can be found from the intersection of several hyperbolic areas. As a result, probability maps for the emitter locations are obtained. In Figure 15, the probability maps obtained from two receivers R_1 and R_2 are shown, for a certain TDOA and different receiver arrangements and frequencies. The greyscale images represent the probability values between 0 (black, low probabilities) and 1 (white, high probabilities) for the corresponding points in the $z = 0$ plane. In Figure 15(a), the receivers are close together, and the frequency is 50 kHz. It can be seen that the white lobes in this case are very wide and the area with the highest probability for the emitter location is bigger and the resolution is worse than before. Figure 15(b) shows the probability map for the emitter location when the distance between the receivers is increased, the frequency remains unchanged at $f = 50$ kHz. Keeping the receivers at the same distance, but increasing the frequency to $f = 300$ kHz reduces the area with the highest probability for the emitter location, as shown in Figure 15(c). In general, the maximum likelihood regions for the emitter location diverge (rather wide lobes) with distance from the receivers and converge (narrower lobes) with higher frequencies and if the two receivers are farther apart from each other.
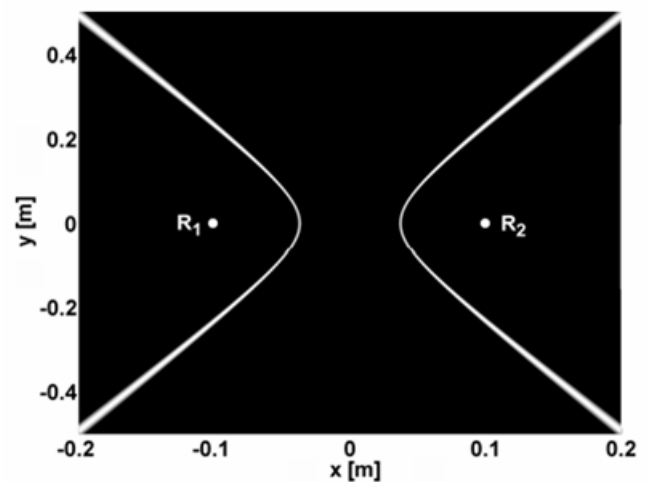
In Figure 16, the probability map for the emitter location in 2-D is shown, if three receivers R_1, R_2 and R_3 are used and the TDOA between all combinations of three receivers to pairs is considered. The x- and y-axis are normalised with the wavelength λ and, therefore, the figure is valid for both $f = 50$ kHz and $f = 300$ kHz. The three emitters are in a distance of 28λ to each other which is about 83 cm at 50 kHz and 14 cm at 300 kHz. This distance is larger and, thus, the lobes are narrower than in Figure 15(b), but it is smaller and, therefore, the lobes are slightly wider than in Figure 15(c). The highest probability value can be found at $x = -5\lambda$ and $y = 3\lambda$ which is the intersection of the three lobes. The intersection is our estimate for the emitter location. The size of this intersection area is an indication for the resolution of the localisation.
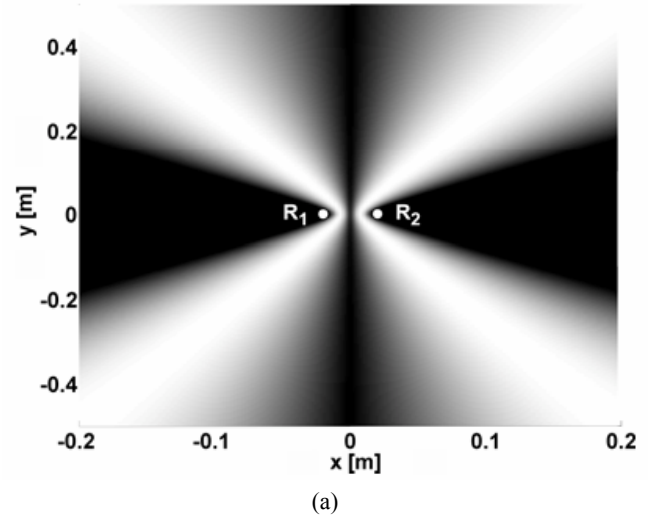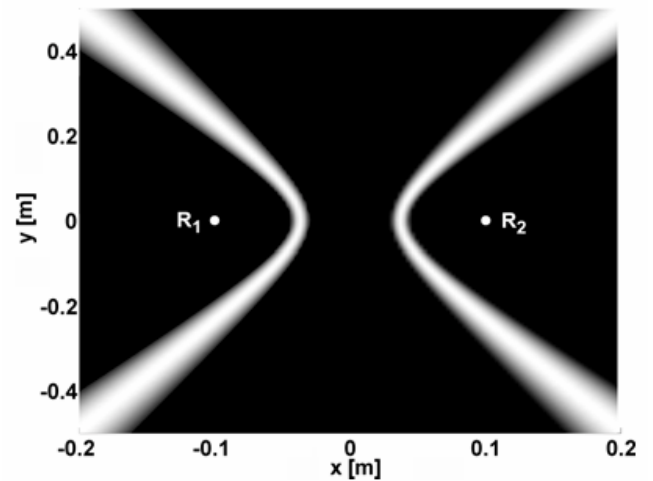
Figure 16 Emitter localisation probability map in 2-D
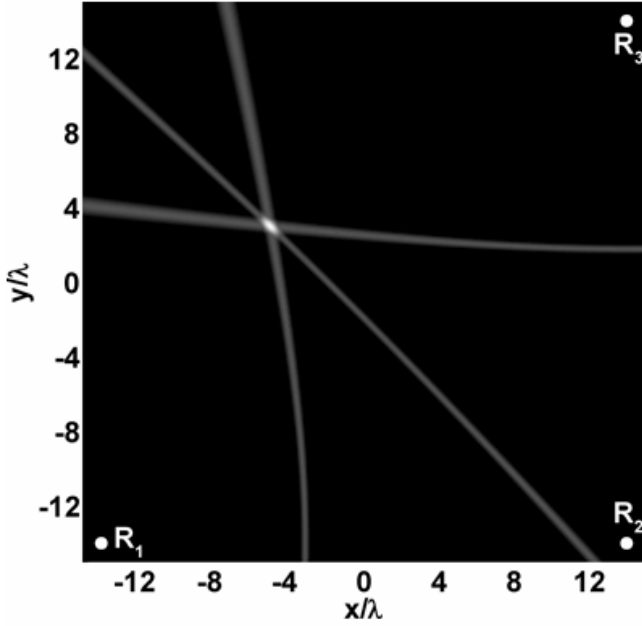
Flückiger et al. (2008) used the radius R^* of the area with the highest localisation probability above a certain threshold as a measure for the localisation resolution. R^* does not depend on the frequency of the emission and can, therefore, be scaled with λ. Figure 17 shows the ratio R^*/λ against the distance d/λ between three receivers. It can be seen that R^*/λ reaches a constant level for about $d \geq 30\lambda$. If the three hydrophones are in a distance of $d = 30\lambda \approx 15$ cm at a frequency of $f = 300$ kHz, then the resolution based on R^* is less than 1 mm.

Figure 17 Expected resolution based on R^* against the distance d between the receivers
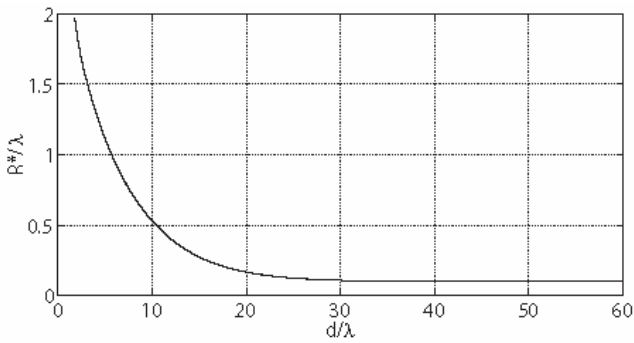
By increasing the ultrasound frequency, the spatial resolution can be increased as well. The penetration depth then becomes a limiting factor, because of the frequency-dependent attenuation of sound. At a frequency of 200 MHz, a resolution of 12 to 14 μm can be achieved, at a penetration depth of usually less than 600 μm. At an ultrasound frequency of 3 GHz, the wavelength is 500 nm, and a scanning acoustic microscope can provide the same resolution as an optical microscope.

Finally, we present a wireless acoustic emitter that has the potential to act as the ultrasonic emitter required for the localisation method described above. Figure 18 shows the schematics of the emitter. It consists of two parallel soft-magnetic (nickel) square dies (facing area of $1 \times 1\text{mm}^2$, thickness $t_{Ni} = 50$ μm) separated by a 125 μm thick plastic shim. One of the plates, the resonator, is suspended on two gold beam springs (thickness $t_{Au} = 29$ μm), the other one is fixed to the gold base frame of the device. The two parts are fabricated separately and then glued together in the microassembly system presented by Probst et al. (2007), with the spacing layer between them.
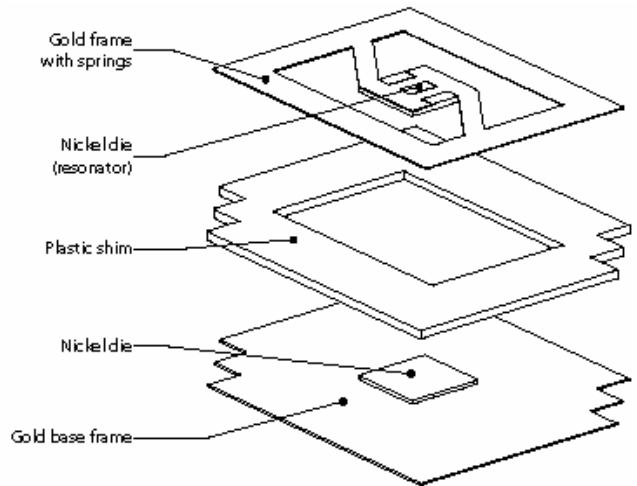
Figure 18 Schematic design

Figure 19 shows the working principle of the wireless emitter. When it is placed in a magnetic field **H**, the soft-magnetic dies become magnetised and an attractive or repulsive force $\mathbf{F}_z$ between the dies is generated, causing the suspended nickel die to move and the gold springs to deflect. Exciting the structure at resonance results in a continuous vibration, acting as a source for pressure waves inside the surrounding fluid.

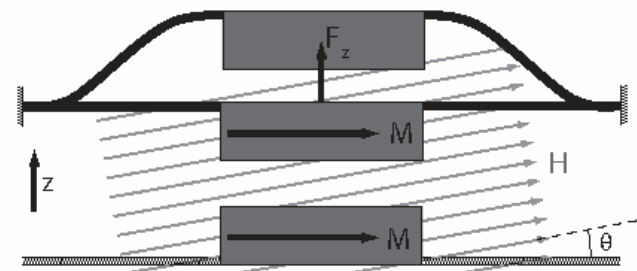**Figure 19** Working principle of the wireless acoustic emitter

Figure 20 shows a sketch of the experimental setup. The emitter is glued to the wall of a container that is filled with water or glycerine. The driving coil is placed below the container (A, corresponding to $\theta = 0°$) or at the wall of the container (B, $\theta = 90°$), such that the emitter lies on the axis of the coil. The magnetic field of the coil excites the resonator close to its first measured resonance mode at $f_1 = 4.125$ kHz. The pressure wave generated by the emitter

relative to the ambient pressure is picked up by a hydrophone placed at 1 cm from the emitter. The hydrophone is a cubic piezo stack with 2 mm side length made from lead zirconium titanate and sealed with silicone rubber. The pressure change recorded at the hydrophone is bandpass filtered, amplified and transferred back to the PC.

Figure 20 Experimental setup (see online version for colours)
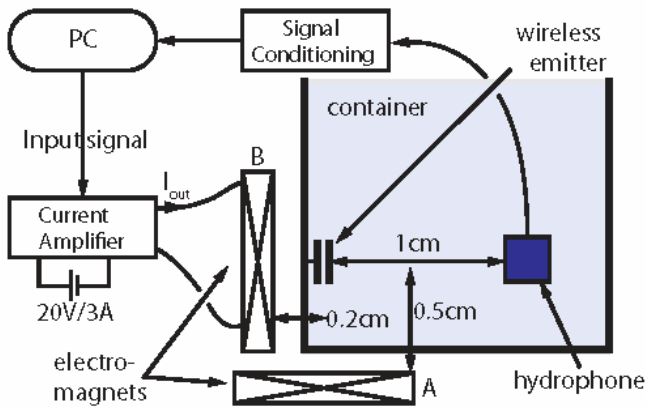
Notes: The electromagnet (coil) A ($\theta = 0°$) or B ($\theta = 90°$) excites the acoustic emitter close to its first mode f_1. The pressure signal is picked up by a hydrophone and transmitted to the PC.

Water is selected as a fluid because it has similar acoustic properties to human tissue, e.g., the speed of sound in water and fat is very similar. To represent tissue like muscles, where the speed of sound is higher, glycerine is used. Figure 21 shows the experimental results for water and glycerine as well as the two coil positions, compared to the theoretical prediction of the pressure presented by Nagy et al. (2009). The results are normalised to the pressure level at an applied current of 4A. Good agreement is found between the theoretical model and the experiment, and it is found that the emitted pressure follows a quadratic law with respect to the applied current.

Figure 21 Experimental results compared to computed pressure
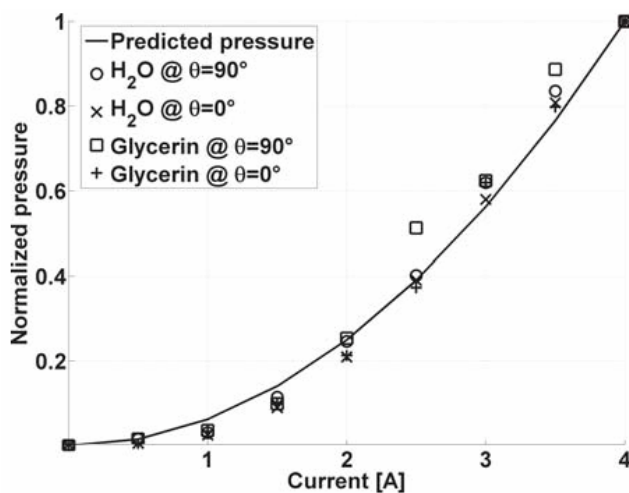
Note: As expected, the pressure is quadratic with the applied current.

The trade-off in the design of the wireless emitter is its natural frequency, which corresponds to the desired frequency of the acoustic signal, versus the signal strength (acoustic pressure). The bigger the area of the nickel dies (for a given thickness), the higher the pressure of the emitted sound wave will be, and the farther from the device a signal can be measured. Yet, at the same time, its resonant frequency will decrease as its mass increases. The current prototype emits acoustic waves in the kHz range, and careful design and fabrication allows us to tune the frequency into the desired frequency range for localisation.

To conclude, the frequency of the emission as well as the amount and the arrangement of the receivers affect the spatial resolution of the emitter localisation. The spatial accuracy of the localisation also depends on accurate time measurements and on a precise knowledge of the speed of sound in the media.

6 Conclusions

In this paper, we introduce the concept of modular robotics for surgical robotics for the GI tract. We presented our studies in the key technologies of self-assembly, actuation, powering, and localisation. The proposed concept has the potential to change the traditional way surgical and diagnostic tasks in the GI tract are performed, and also to create a new set of procedures currently not available.

References

Abbott, D., Becke, C., Rothstein, R., and Peine, W. (2007) 'Design of an endoluminal notes robotic system', in *Proc. IEEE/RSJ Int. Conf. Intelligent Robots and Systems*, pp.410–416.

ARES website (2009) 'The ARES (assembling reconfigurable endoluminal surgical system)', Project website, available at http://www.ares-nest.org.

Carta, R., Lenaerts, B., Thone, J., Tortora, G., Valdastri, P., Menciassi, A., Puers, R. and Dario, P. (2008) 'Wireless power supply as enabling technology towards active locomotion in capsular endoscopy', in *Eurosensors 2008*, Dresden.

Catrysse, M., Hermans, B. and Puers, R. (2004) 'An inductive power system with integrated bi-directional data-transmission', *Sensors and Actuators A-Physical*, Vol. 115, Nos. 2–3, pp.221–229.

Flückiger, M., Neild, A. and Nelson, B.J. (2008) 'Optimization of receiver arrangements for passive localization methods. *Ultrasonics*, Submitted.

Flückiger, M. and Nelson, B.J. (2007) 'Ultrasound emitter localization in heterogeneous media', in *Proc. IEEE Int. Conf. of the Engineering in Medicine and Biology Society*, pp.2867–2870.

Harada, K., Susilo, E., Pak, N.N., Menciassi, A. and Dario, P. (2008) 'Design of a bending module for assembling reconfigurable endoluminal surgical system', in *Proc. 6th Int. Conf. Int. Soc. Gerontechnology (ISG-08)*, Pisa, Italy, pp.ID–186.

Hoover, A.M., Steltz, E. and Fearing, R.S. (2008) 'RoACH: an autonomous 2.4g crawling hexapod robot', in *Proc. IEEE/RSJ Int. Conf. Intelligent Robots and Systems*, Nice, France, pp.26–33.

Lehman, A., Wood, N., Dumpert, J., Oleynikov, D. and Farritor, S. (2008) 'Robotic natural orifice translumenal endoscopic surgery', in *Proc. IEEE Int. Conf. Robotics and Automation*, pp.2969–2974.

Lenaerts, B. and Puers, R. (2005) 'Inductive powering of a freely moving system', *Sensors and Actuators A: Physical*, Vols. 123–24, pp.522–530.

Menciassi, A., Valdastri, P., Harada, K. and Dario, P. (2008) 'Single and multiple robotic capsules for endoluminal diagnosis and surgery', in *Proc. IEEE/RASEMBS Int. Conf. Biomedical Robotics and Biomechatronics*, Arizona, USA.

Nagy, Z., Abbott, J.J. and Nelson, B.J. (2007) 'The magnetic self-aligning hermaphroditic connector: a scalable approach for modular microrobots', in *IEEE/ASME Int. Conf. Advanced Intelligent Mechatronics*.

Nagy, Z., Fluckiger, M., Ergeneman, O., Pane, S., Probst, M. and Nelson, B.J. (2009) 'A wireless acoustic emitter for passive localization in liquids', in *Proc. IEEE Int. Conf. Robot. Automat.*, Kobe, Japan.

Nagy, Z., Oung, R., Abbott, J.J. and Nelson, B.J. (2008) 'Experimental investigation of magnetic self-assembly for swallowable modular robots', in *Proc. IEEE/RSJ Int. Conf. Intelligent Robots and Systems*, pp.1915–1920.

O'Handley, R.C., Huang, J.K., Bono, D.C. and Simon, J. (2008) 'Improved wireless, transcutaneous power transmission for in vivo applications', *IEEE Sensors J.*, Vol. 8, No. 1, pp.57–62.

Peirs, J., Reynaerts, D. and Van Brussel, H. (1998) 'Scale effects and thermal considerations for micro-actuators', in *Proc. IEEE Int. Conf. Robot. Automat.*, Vol. 2, pp.1516–1521.

Probst, M., Borer, R. and Nelson, B.J. (2007) 'A microassembly system for manufacturing hybrid mems', in *Proc. of the 12th IFToMM World Congress*, Besancon, France.

Quirini, M., Menciassi, A., Scapellato, S., Stefanini, C. and Dario, P. (2008) 'Design and fabrication of a motor legged capsule for the active exploration of the gastrointestinal tract', *IEEE/ASME Trans. Mechatronics*, Vol. 13, pp.169–179.

Ryu, M., Kim, J.D., Chin, H.U., Kim, J. and Song, S.Y. (2007) 'Three-dimensional power receiver for in vivo robotic capsules', *Medical & Biological Engineering & Computing*, Vol. 45, No. 10, pp.997–1002.

Sendoh, M., Ishiyama, K. and Arai, K. (2003) 'Fabrication of magnetic actuator for use in a capsule endoscope', *IEEE Trans. Magnetics*, Vol. 39, No. 5, pp.3232–3234.

Susilo, E., Valdastri, P., Menciassi, A. and Dario, P. (2008) 'A miniaturized wireless control platform for robotic capsular endoscopy using pseudokernel approach', in *Proc. Eurosensors 2008*, Dresden.

Wells, P.N.T. (2000) 'Current status and future technical advances of ultrasonic imaging', *IEEE Engineering in Medicine and Biology Magazine*, Vol. 19, pp.14–20.

Wood, R.J., Avadhanula, S., Sahai, R., Steltz, E. and Fearing, R.S. (2008) 'Microrobot design using fiber reinforced composites', *Journal of Mechanical Design*, Vol. 130, No. 5, pp.052304(1–11).